J Digit Imaging (2014) 27:824–832
DOI 10.1007/s10278-014-9707-y

Pilot Study: Evaluation of Dual-Energy Computed Tomography Measurement Strategies for Positron Emission Tomography Correlation in Pancreatic Adenocarcinoma

Jorge Oldan · Miao He · Teresa Wu · Alvin C. Silva · Jing Li · J. Ross Mitchell · William M. Pavlicek · Michael C. Roarke · Amy K. Hara

Published online: 4 July 2014

Abstract We sought to determine whether dual-energy computed tomography (DECT) measurements correlate with positron emission tomography (PET) standardized uptake values (SUVs) in pancreatic adenocarcinoma, and to determine the optimal DECT imaging variables and modeling strategy to produce the highest correlation with maximum SUV (SUV_{max}). We reviewed 25 patients with unresectable pancreatic adenocarcinoma seen at Mayo Clinic, Scottsdale, Arizona, who had PET–computed tomography (PET/CT) and enhanced DECT performed the same week between March 25, 2010 and December 9, 2011. For each examination, DECT measurements were taken using one of three methods: (1) average values of three tumor regions of interest (ROIs) (method 1); (2) one ROI in the area of highest subjective DECT enhancement (method 2); and (3) one ROI in the area corresponding to PET SUV_{max} (method 3). There were 133 DECT variables using method 1, and 89 using the other methods. Univariate and multivariate analysis regression models were used to identify important correlations between DECT variables and PET SUV_{max}. Both R^2 and adjusted R^2 were calculated for the multivariate model to compensate for the increased number of predictors. The average SUV_{max} was 5 (range, 1.8–12.0). Multivariate analysis of DECT imaging variables outperformed univariate analysis (r=0.91; R^2=0.82; adjusted R^2=0.75 vs r<0.58; adjusted R^2<0.34). Method 3 had the highest correlation with PET SUV_{max} (R^2=0.82), followed by method 1 (R^2=0.79) and method 2 (R^2=0.57). DECT thus has clinical potential as a surrogate for, or as a complement to, PET in patients with pancreatic adenocarcinoma.

Keywords Cancer · Dual-energy CT · Informatics · Pancreas · Pancreatic adenocarcinoma · PET · PET/CT

Abbreviations

CfsSubsetEval	Correlation-based feature subset selection evaluation
CT	Computed tomography
DECT	Dual-energy computed tomography
PA	Pancreatic adenocarcinoma
PET	Positron emission tomography
ROI	Region of interest
SUV	Standardized uptake value
SUV_{max}	Maximum standardized uptake value
VIF	Variance inflation factor

Introduction

Single-energy computed tomography (CT) is commonly used for the diagnosis, staging, and follow-up of patients with pancreatic cancer [1]. Single-energy CT utilizes Hounsfield unit attenuation of lesions to infer tumor viability. These attenuation measurements, however, can be inaccurate due to volume averaging, beam hardening, or the presence of high-density blood products, protein, or calcification [2]. Although positron emission tomography (PET) is generally not as effective as CT for locoregional and nodal staging of pancreatic cancer [3], it can be used for preoperative diagnosis of pancreatic adenocarcinoma (PA) when CT and/or biopsy are nondiagnostic or when the patient has concurrent chronic

J. Oldan · A. C. Silva · J. R. Mitchell · W. M. Pavlicek · M. C. Roarke · A. K. Hara (✉)
Department of Radiology, Mayo Clinic, 13400 E Shea Blvd, Scottsdale, AZ 85259, USA
e-mail: hara.amy@mayo.edu

M. He · T. Wu · J. Li
School of Computing, Informatics, and Decision Systems Engineering, Arizona State University, Tempe, AZ, USA

pancreatitis and/or cystic tumors. It can also be used for detection of distant metastases, for differentiation of radiation-induced fibrosis from tumor recurrence, and, according to some preliminary findings, for monitoring of therapy [4, 5]. PET, however, is expensive, time-consuming, and less widely available than CT.

Dual-energy CT (DECT) is an imaging technique approved by the US Food and Drug Administration that uses two different energies (usually 80 and 140 kVp) instead of a single energy to produce CT images. Scanning at different radiographic energies facilitates differentiation of materials such as calcium, uric acid, iodine, and water, which can be helpful in various clinical applications (e.g., evaluating renal stone composition [6, 7] or differentiating cysts from solid tumors [8]). Specifically, in cases of PA, DECT has shown excellent differentiation of tumors from normal pancreas [9], and it may even allow for the elimination of noncontrast acquisition [10]; the DECT technology, by separating out the iodine-loaded images, allows one to generate a "virtual noncontrast" image. Intravenous contrast is still necessary. Recently, high correlation was demonstrated between positron emission tomography (PET) maximum standardized uptake value (SUV_{max}) and DECT iodine values in nonsmall-cell lung cancer [11]. If high correlations between DECT and PET signals are observed in other cancers, then DECT may reduce the need for more costly and time-consuming PET imaging.

The purpose of this study was to determine which DECT imaging variables and which modeling strategy would produce the highest correlation with PET SUV_{max} in patients with unresectable PA.

Materials and Methods

This retrospective study was approved by the Mayo Clinic Institutional Review Board, which waived the need for signed, informed consent because this retrospective review was deemed minimal risk.

Patient Selection

Inclusion criteria included a diagnosis of pathologically proven unresectable PA and PET/CT and contrast-enhanced DECT conducted within the same week between March 25, 2010 and December 9, 2011. All patients were adults.

A total of 25 patients with a diagnosis of PA were identified who met study criteria: 17 men and 8 women, with a mean age of 65 years (range, 50–81 years). The average time between PET and DECT was 1 day (range, 0–7 days). The mean maximum axial diameter of the lesions was 4.3 cm (range, 1.5–8.4 cm). Pancreatic cancers were located in the uncinate process (n=4), the head (n=7), the neck/body (n=10), and the tail (n=8) (some cancers were present in more than one region). All patients had unresectable or metastatic disease at the time of DECT. Of the 25 patients, 13 had hepatic metastases, 12 had nodal metastases, and 21 had vascular involvement of the mesenteric vessels or portal vein. All had pathologically proven PA.

CT Protocol

All DECT examinations were performed as part of a standard biphasic pancreatic CT protocol on a 64-slice single-source DECT scanner with fast kilovolt switching (CT750 HD; GE Healthcare, Milwaukee, Wisconsin). This protocol consisted of a single-energy pancreatic phase (approximately 40 s after injection of a contrast agent) and a dual-energy portal venous phase (70 s after injection of contrast), using a body weight-based volume (1 mL/kg) of low molecular weight, nonionic, iodinated contrast medium at 4 mL/s. Specific imaging parameters are shown in Table 1. The DECT portal venous data produced monochromatic images from 40 to 140 keV, and iodine and water (virtual precontrast) basis pairs, as well as other basis pairs (eg, calcium–iodine) more commonly used for other applications such as distinguishing kidney stones.

PET Protocol

All PET scans were performed on a combined 16-slice PET/CT scanner (GE Discovery 600 PET/CT; GE Healthcare) within 7 days of the DECT scan. The PET scan used 3.27-mm slices and a three-dimensional acquisition with the VUE Point HD reconstruction filter. Image matrix was 192× 192 pixels. A total of seven to nine 15-cm bed positions were acquired at 2 min per bed position if body mass index was <35 or at 3 min per bed position if body mass index was ≥35. A simultaneous noncontrast CT was performed at 120 kVp, 100 mA to 120 mA, nonhelical, with 3.75-mm slice thickness. Coregistration between PET and noncontrast CT was performed using MIMvista software (MIMvista 5.2.3; MIM

Table 1 Pancreatic and venous phase protocols

Series	Speed, mm/rot	Pitch	Collimation, mm	Slice thickness, mm	Reconstruction interval, mm	kVp	Min/max, mA
Pancreatic	39.38	0.98	0.625	2.50	2	120	150–450
DECT venous	39.38	0.98	0.625	3.75	3	80,140	630

DECT dual-energy computed tomography, *Max* maximum, *Min* minimum, *rot* rotation

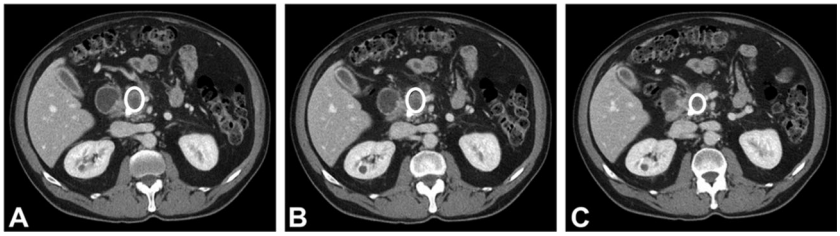

Fig. 1 Pancreatic adenocarcinoma regions of interest on CT. Method 1 used three regions of interest (**a**–**c**, *circles*) in separate areas of tumor heterogeneity, each in a different slice

Software Inc., Cleveland, Ohio). The PET SUV_{max} within the tumor was used for analysis.

DECT Region of Interest Selection

All DECT monochromatic images were sent to an offline computer workstation (GE Advantage Workstation, version 4.5; GE Healthcare) for image analysis using a commercially available viewer software (Gemstone Spectral Imaging Viewer, version 2.0; GE Healthcare).

In this study, three different DECT measurement methods (method 1, method 2, and method 3) were evaluated. All regions of interest (ROIs) were placed by a single board-certified radiologist (J.O.) for this early pilot study. For method 1, a total of three ROIs were manually drawn in three different locations of tumor heterogeneity in the solid enhancing tumor on the DECT images (Fig. 1). The three different slices were selected manually to be within the substance of the tumor in areas that appeared visually similar to the rest of the tumor and were located on different image slices. For method 2, a single ROI was drawn in the area of the tumor with the highest visible DECT enhancement (Fig. 2a). For method 3, a single ROI was drawn at DECT (Fig. 2b) in the area of the tumor corresponding to the highest PET SUV_{max} (Fig. 2c). Each ROI covered as much tumor as possible without including adjacent vessels or structures. The observer had access to the PET/CT scanner at the time of ROI selection, but it was not used for methods 1 and 2.

DECT Measurements

Methods 1, 2, and 3 provided 133, 89, and 89 variables, respectively, for analysis (Table 2). These included means, minima, maxima, and SDs of ROIs generated using different basis pairs (of which there were 5 pairs of materials, producing 10 sets of images, and 1 for effective Z, or atomic number) and keV settings (of which there were 11, from 40 to 140 keV in 10-keV increments). Methods 2 and 3 produced four variables to analyze (mean, minimum, maximum, and SD), and method 1 produced six variables (as both maxima and minima could be either the maximum or the minimum of the three ROIs, or their average). Each method included a variable for the patient's mass, which impacts standardized uptake value (SUV):

$$\mathrm{SUV}\left(\mathrm{g}/\mathrm{mL}\right) = \frac{\mathrm{local\,concentration}\left(\mathrm{g}/\mathrm{mCi}\right)}{\mathrm{injected\,dose(mCi)}/\mathrm{weight(g)}}$$

The analysis software saved all data to Excel (Microsoft Inc; Redmond, Washington) files at every kiloelectronvolt in 10-keV increments from 40 to 140 keV. There were multiple CT data sets, but the radiologist only drew his ROIs on the standard 70 keV data set. Since the images are reconstructed from the same pair of high-energy and low-energy images, which are perfectly registered because they are acquired at the same time, the ROI is simultaneously applied to all data sets. Measurements were reported in Hounsfield units for monochromatic kiloelectronvolt images and in microgram per milliliter (iodine) and milligrams per milliliter (water) for basis pairs.

Statistical Analysis

Univariate analysis was conducted first to determine the correlation between each DECT variable and PET SUV_{max}.

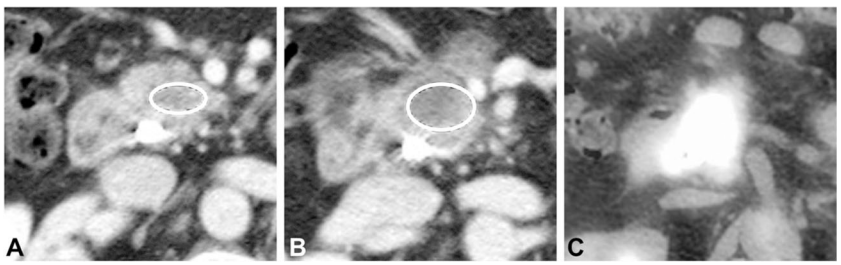

Fig. 2 Regions of interest on methods 2 and 3 (CT and PET/CT). **a** Region of interest corresponding to maximum computed tomography (CT) attenuation. **b** Region of interest corresponding to maximum positron emission tomography (PET). **c** PET of the same tumor. All images are from the same patient

Table 2 Differences among region-of-interest placement methods and the total number of DECT variables measured

	Method 1[a]	Method 2	Method 3
No. of DECT ROIs used	Three ROIs in areas of the greatest tumor heterogeneity (variables averaged across all three)	One ROI corresponding to the highest CT attenuation	One ROI corresponding to area of the highest SUV_{max}
No. of image contrasts	22 Images: 1 effective Z image + 11 keV images (40–140 keV in 10-keV increments) + 10 material images: two images per basis pair × five basis pairs: (1) I-water, (2) Ca-I, (3) Ca-water, (4) HAP-I, and (5) HAP-Ca		
No. of variables measured per image contrast	Six variables: mean, SD, mean–max, mean–min, max–max, min–min	Four variables: mean, SD, max, min	
Total No. of DECT variables	133 Variables: (22 image contrasts × 6 variables per contrast) + mass	89 Variables: (22 image contrasts × 4 variables per contrast) + mass	

Ca calcium, *CT* computed tomography, *DECT* dual-energy computed tomography, *HAP* hydroxyapatite, *I* iodine, *max* maximum, *min* minimum, *ROI* region of interest, *SUV* standardized uptake value

[a] In method 1, three ROIs were measured, resulting in three maxima and three minima. "Max–max" refers to the highest of the three maxima, "mean–max" to their arithmetic mean. Similarly, "min–min" is the lowest of the three minima, whereas "mean–min" is their arithmetic mean

Multivariate analysis was then performed to jointly consider the predictive power of multiple features. Because of the large number of DECT variables, we used Weka 3.2 (Waikato Environment for Knowledge Analysis, University of Waikato, Hamilton, New Zealand) [12], an open-source machine-learning software, for variable selection. This process may improve the interpretation and predictive accuracy of statistical model development [13]. A linear forward feature selection method (using the linear forward feature selection option from the CfsSubsetEval [correlation-based feature subset selection evaluation] method within Weka) was applied to select subsets from the original DECT variables by removing uncorrelated, redundant, and noisy data. A list of features was then selected in order of importance for correlation with SUV_{max}.

For each ROI method, the statistical modeling software Minitab 16 (Minitab Inc; State College, Pennsylvania) was used to model the correlations between the SUV_{max} and the selected variable subsets. Addressing the issue of potential multicollinearity among the selected features was done by developing a forward statistical model by adding one feature at a time. The variance inflation factor (VIF) was then calculated to assess possible correlations between features. VIF is a common index for measuring the severity of multicollinearity in statistical models, and VIF >10 indicates that a model has multicollinearity issues [2]. Using this guideline, we developed the regression models for first order, second order, and second order with interaction effects. For model performance, we calculated both R^2 and adjusted R^2.

R^2, also known as the coefficient of determination, is a measure of the proportion of the total variation in a variable that is explained by a given model. It is defined as

$$R^2 \equiv 1-(SS_{res}/SS_{tot})$$

where

$$SS_{tot} = \sum_i (y_i - \bar{y})^2 \text{ and } SS_{res} = \sum_i (y_i - f_i)^2$$

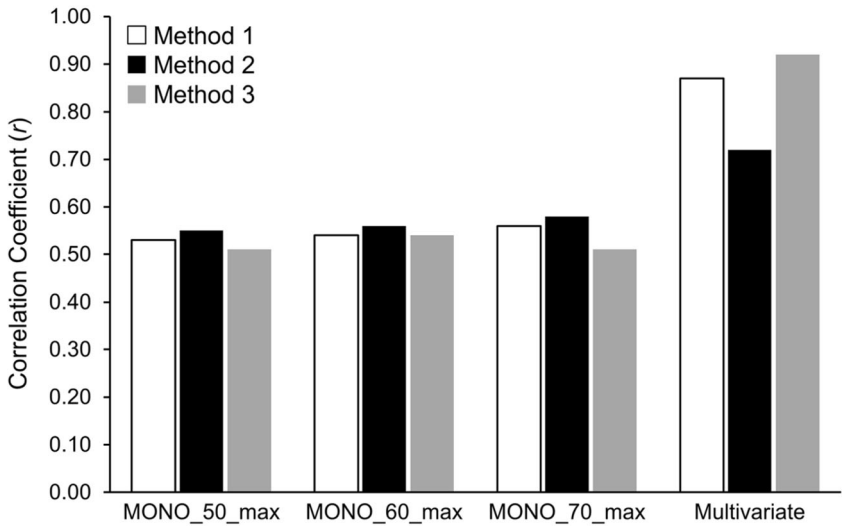

Fig. 3 Multivariate and univariate correlations. Multivariate analysis of methods 1 to 3 outperformed the highest correlations with univariate analysis. MONO_50_max, MONO_60_max, and MONO_70_max refer to maxima at 50 keV, 60 keV, and 70 keV, the best correlated single variables

where "y_i" is each individual observation, "f_i" is the predicted observation due to the model, and "$\bar{y}$" is the overall mean of all observations.

Adjusted R^2 is meant to counterbalance the tendency of R^2 to rise as additional predictors are added. Adjusted R^2 is defined as

$$\text{Adjusted}\,R^2 = R^2 - \left(1-R^2\right)p/(n-p-1)$$

where "n" is the sample size and "p" is the number of predictors.

R^2 is known to increase with the addition of predictors to the model, whereas adjusted R^2 compensates for the number of predictors and thus adjusts for this inflation. For comparison purposes, we transformed R^2, obtained from the multivariate regression models, to r to compare against the performance of univariate analysis.

The "r" is the coefficient of correlation between two variables, measuring the strength of a linear association. It is calculated as

$$r = \left(\sum_i (X_i-\overline{X})(Y_i-\overline{Y})\right) \Big/ \left(\sqrt{\sum_i (X_i-\overline{X})^2}\sqrt{\sum_i (Y_i-\overline{Y})^2}\right)$$

for a single variable, $R^2=r^2$.

Results

DECT and PET/CT Correlation Results

Univariate modeling resulted in only three DECT variables (the maximum values of 50, 60, and 70 keV monochromatic) with a correlation of $r>0.50$ with SUV_{max}. The greatest of these was $r=0.58$. Multivariate analysis of DECT imaging variables outperformed univariate analysis (Fig. 3), achieving $r=0.91$ ($R^2=0.82$) compared to $r=0.58$ ($R^2=0.34$) with univariate analysis. Table 3 lists the R^2 between DECT variables and SUV_{max} for the three different ROI methods and multivariate modeling strategies. For each ROI placement method, the most complex modeling strategy (second order with interactions) produced the highest correlations. Overall, the highest correlation obtained between DECT variables and SUV_{max} was found in method 3 ($R^2=0.82$), followed by method 1 ($R^2=0.79$) and method 2 ($R^2=0.57$). The area of highest PET SUV and of highest visible DECT enhancement correlated in 20 of the 25 cases.

The DECT variables that correlated best with SUV_{max} from method 3 ($P<0.05$) are shown in Table 4. In addition, the coefficient, P value, and VIF are provided. The first order, the second order, and the second order with interactions models included 3, 6, and 7 variables, respectively. As shown in Table 4, all predictors in the three models proved to be significant ($P<0.05$). In addition, when a predictor had VIF <10, it had relatively little correlation with other predictors (although not necessarily no correlation).

Since method 3 requires the use of PET/CT to fully investigate the clinical use of DECT as a surrogate for PET/CT, we report the best model (second order with interactions) from method 1, which provides comparable results to those from method 3 (Table 5). We observed high multicollinearity among the features, both in method 1 and in method 2. Although reports in the medical literature indicate that multicollinearity does not reduce the predictive power of the model as a whole [14], it does increase the standard errors of estimates of the coefficients, thus complicating interpretation of the model. To remove multicollinearity from the model, we first identified the highly correlated features as a group, then introduced a novel composite feature (as described in Table 5) as a linear combination of the correlated features. As a result, the regression model showed $R^2=0.79$ and adjusted $R^2=0.75$, with all predictors (including the composite feature) being significant ($P<0.05$) with VIF <10.

Optimal Models

Optimal models themselves are as follows. For method 3, the optimal first-order model was the following:

$$\begin{aligned}\text{SUV}_{max} = {} & 0.029 \times 90\ \text{keV mean} - 0.017 \times \text{iodine calcium min} \\ & + 0.019 \times \text{weight}\end{aligned}$$

The optimal second-order model was the following:

$$\begin{aligned}\text{SUV}_{max} = {} & 0.024 \times 90\ \text{keV mean} - 0.025 \times \text{iodine calciummin} \\ & + 0.024 \times \text{iodinecalciummax} - 0.116 \times \text{iodine water SD} \\ & + 0.00185 \times \text{calcium iodine max}^2 + 0.0016243 \\ & \times 90\text{keVmean}^2\end{aligned}$$

The optimal second-order model with interactions was the following:

$$\begin{aligned}\text{SUV}_{max} = {} & 0.026 \times 90\ \text{keV mean} - 0.0142 \times \text{iodine calciummin} \\ & + 0.0107 \times \text{iodine calciummax} + 0.01 \times \text{weight} \\ & + 0.00162 \times \text{calcium iodinemax} \times \text{weight} + 0.00147 \\ & \times 90\ \text{keV mean} \times \text{iodine calciummin} - 0.000605 \\ & \times \text{iodine calcium max}^2\end{aligned}$$

Table 3 Summary of the coefficient of determination (R^2) for the three ROI placement methods and different models

ROI placement	No. of variables	First-order model	Second-order model	Second-order model with interactions
Method 1	133	0.65	0.76	0.79
Method 2	89	0.36	0.36	0.57
Method 3	89	0.55	0.68	0.82[a]

ROI region of interest

[a] The best result (highest correlation) in each row and column was using method 3

For method 1, the optimal model was the following:

$$\begin{aligned}\mathrm{SUV_{max}} = {} & 9.871 \times \text{effective ZSD} - 0.001608 \times \text{100 keV meanmax} \\ & \times \text{140 keVmeanmax} - 0.12867 \times \text{140 keV meanmax} \\ & \times \text{effectiveZ meanmax} + 0.751 \times \text{composite}\end{aligned}$$

with the composite defined as in Table 5.

Discussion

The first goal of this study was to identify the correlations between DECT variables obtained via three different measurement methods and PET $\mathrm{SUV_{max}}$. Method 3 provided the highest correlation (R^2=0.82) between DECT variables and PET signal, which is not surprising since DECT data were obtained at the site of maximal fluorine 18 (^{18}F) fluorodeoxyglucose uptake. However, it required manually coregistered DECT and PET scans. In clinical practice, a PET scan may not always be available or desired. In that case, method 1, which required three ROIs in the area of greatest tumor heterogeneity in the DECT scan, performed nearly as well (R^2=0.79). Conversely, method 2, a single ROI in the area of highest DECT enhancement, was not as effective (R^2= 0.57), although the selected variables overlapped considerably, with measurements corresponding to $\mathrm{SUV_{max}}$.

As a result, in order to make maximum use of DECT results to properly model the effects of PET/CT without performing a PET/CT scan, it may be necessary to take multiple

Table 4 Multivariate models for method[a,b]

	Features	Coefficient	*P* value	VIF
First-order model	*90 keV mean*	0.029	0.006	1.207
R^2=0.55	*Iodine–calcium min*	−0.017	0.04	1.080
R^2 (adjusted)=0.39	BMI	0.019	0.005	1.144
Second-order model	*90 keV mean*	0.024	0.008	1.269
R^2=0.68	*Iodine–calcium min*	−0.025	0.01	1.944
R^2 (adjusted)=0.57	Iodine–calcium max	0.024	0.01	2.912
	Iodine–water SD	−0.116	0.047	4.812
	Calcium–iodine max ^2	0.00185	0.01	1.582
	90 keV mean ^2	*0.0016243*	0.01	1.079
Second-order model with interactions	*90 keV mean*	0.0263	0.001	1.38
R^2=0.82	*Iodine–calcium min*	−0.0142	0.02	1.30
R^2 (adjusted)=0.75	Iodine–calcium max	0.0107	0.04	1.63
	Weight	0.0100	0.047	1.70
	Calcium–iodine max × weight	0.00162	0.001	1.38
	90 keV mean × iodine–calcium min	0.00147	0.02	1.20
	Iodine–calcium max ^2	−0.000605	0.02	1.51

The significant value $p<0.05$

BMI body mass index, *max* maximum, *min* minimum, *VIF* variance inflation factor

[a] Pairs of substances represent the use of proprietary software designed to separate a pair of substances. For example, the iodine–calcium min is the lowest value pixel (minimum) on an image designed to separate iodine from calcium. On such an image, iodine will have higher values and calcium will have lower values. Conversely, on the calcium–iodine images, calcium will have higher values and iodine will have lower values. "Effective Z" refers to an image where the value is an estimate of the effective atomic number (Z); on these images, iodine will be higher than calcium, which will, in turn, be higher than the hydrogen, oxygen, nitrogen, and carbon that make up most of human tissue

[b] Variables in italics are used in all three regression models

measurements of the tumor, as we did in method 1 when drawing three ROIs, to reflect the heterogeneity of the tumor. This may reflect linkage between tumor heterogeneity and metabolic activity, as hypothesized below. Although we observed high correlations among the measures using this approach (and method 2), the use of composite features formed by aggregating the highly correlated features (Table 5) enabled us to identify the regression model with interpretability.

With univariate analysis, the best single DECT predictors that correlated with PET SUV_{max} (the ROI maxima at 50, 60, and 70 keV) were from lower energy levels (in this study, 50, 60, and 70 keV). However, multivariate analysis of DECT imaging predictors significantly outperformed univariate analysis (r=0.91 [R^2=0.82] vs r<0.60 [R^2<0.36]) in our particular model. In other words, analysis using combinations of multiple imaging variables correlated with PET better than using only single variables such as iodine values or a 70-keV monochromatic Hounsfield unit. However, our results were different from those of a prior study of DECT and PET in small cell lung cancer [10] that found a univariate correlation (r=0.88) between SUV_{max} and iodine-related enhancement (equivalent to an iodine–water basis pair). One explanation may be the lower SUVs in pancreatic cancers (mean, 5 [our study]), whereas the aforementioned lung cancer study reported a high mean SUV of 14. Although precise cutoffs vary, an abnormal SUV for pancreatic cancer is considered to be above 2 to 3 [15–18].

The authors of the lung cancer study did not perform multivariate correlation for comparison. Correlation of a single DECT value would be simple to apply in clinical practice, but in pancreatic cancer, it may not be as accurate as more complex multivariate models. The practical clinical application of a multivariate model (e.g., from method 1) will likely require the complexity to be hidden by implementation in an easy-to-use computer program. Such a program could potentially produce a "virtual PET SUV value" in response to placement of a DECT ROI and thus greatly enhance the use of DECT for diagnosis of PA. It is our intention to create a "virtual PET SUV_{max}" as the subject of future research and to test its applicability in the clinical setting.

The second goal of this study was to identify the DECT imaging variables and modeling strategy that produced the highest correlations with SUV_{max}. With method 3, weight was positively correlated with SUV_{max}. The model also showed that some of the most significant variables correlated to images with lower iodine, such as 90 keV (positive correlation) and iodine–calcium minimum (negative correlation). At 90 keV, the image is more heavily weighted toward water because iodine is the brightest at a lower keV (e.g., 40 keV) and lowest at a higher kiloelectronvolt (e.g., 140 keV) (Fig. 4). The exact correlation between the keV and the iodine and water basis pair images is shown in Fig. 5 for a typical ROI. Conversely, the iodine–calcium image would be weighted more heavily toward iodine. The fact that the method 3 model showed a significant negative correlation to an iodine–calcium minimum implies that a lower iodine concentration visualized on DECT correlates with a higher PET SUV. The correlation with images associated with low iodine suggests that precontrast images may be more relevant in pancreatic cancer than previously thought. Although prior CT investigations of the pancreas without intravenous contrast demonstrated no clinically significant difference in noncontrast density [19–21], some authors have noted that PA is denser than healthy tissue [19]. As tumors are effectively treated, they typically become less dense, breaking up the fibrotic stroma, and they become less metabolic. This correlation of low iodine and high PET SUV could indicate that lower Hounsfield unit values at DECT imply denser tissue and correlate with more aggressive or metabolically active PA. If so, that could aid the prognosis or the development of effective treatment strategies not currently available for similar-appearing hypodense PA. In the future, it may be possible to evaluate tumor viability with DECT using this strategy (similar to PET/CT), but larger studies are necessary to confirm this hypothesis.

Table 5 Second-order with interactions model from method 1

	Features	Coefficient	*P* value	VIF
Second-order interaction	Effective_Z SD	9.871	0.001	1.35
R^2=0.79	100 keV meanmax[a] × 140 keV meanmax	−0.001608	0.03	8.43
R^2 (adjusted)=0.75	140 keV meanmax × effective_Z meanmax	−0.12867	0.003	9.59
	Composite[b]	0.7510	<0.001	6.27

VIF, variance inflation factor

[a] The term "meanmax" refers to the mean of the maxima of the three regions of interest (ROIs) drawn. The term "maxmax" refers to the highest of the maxima of the three ROIs drawn (i.e., the highest pixel value among the three ROIs)

[b] Composite = −0.1432981 × 90keV_maxmax + 0.2718076 × 100keV_meanmax + 17.3583 × effective_Z_meanmax −0.458754 × calcium_NaUrate_meanmax −1.167255 × effective_Z_standard deviation × 90 keV_maxmax + 2.309526 × effective_Z_standard deviation × 100keV_meanmax

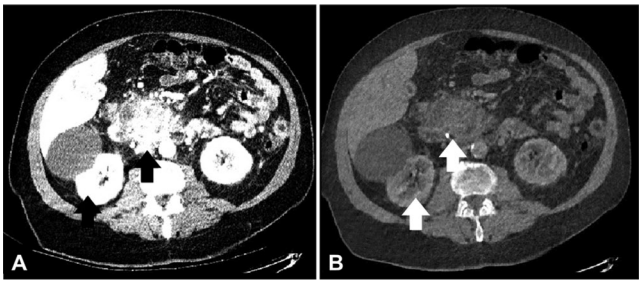

Fig. 4 Pancreatic adenocarcinoma on DECT at different simulated keV levels. Same pancreatic tumor as in Fig. 2 at (**a**) 40 keV and (**b**) 140 keV. Note that, at the lower energy, the iodine attenuation is enhanced (*arrows*). At the higher energy, the water attenuation is dominant, appearing like a precontrast image

Limitations of this study include its retrospective design, use of a single observer, and small sample size (n=25). Replicating this study with a larger sample size and multiple observers would be a logical next step. In addition, the ROIs were placed subjectively, which might have impacted the reproducibility of the results. At the time of this study, no automated or semiautomated software programs were available to measure pancreatic tumors during DECT to decrease measurement variability. Additionally, SD and SUV_{max} are relatively crude measures of heterogeneity; more sophisticated measures of tumor texture, such as those based on the Stockwell transform [22, 23] could be used as well. A more objective measurement approach such as texture analysis may ultimately achieve more reliable and reproducible results than our subjective placement of ROIs; however, these techniques are not currently commercially available. Some authors have already shown the predictive value of baseline texture parameters and resulting changes in chemotherapy for renal cell carcinoma [24]. Similarly, texture analysis has been used to classify lung tumors [25] and head and neck tumors [26], so these techniques might also be useful in pancreatic cancer. Another direction for future study would be to investigate changes in the correlation of DECT with PET/CT over time, looking specifically at patients with high SUVs who are treated with chemotherapy.

Another potential limitation is that reconstruction algorithms might produce different results from different vendor scanners. Our results only represent those from a single vendor scanner (General Electric). Currently, this type of DECT analysis is not automated or routinely available clinically. If these results are confirmed in larger groups of patients, it may be possible to develop a "virtual PET" DECT image or results.

DECT has many potential advantages over PET/CT in terms of imaging time, cost, and spatial resolution that make it an attractive option. DECT image acquisition takes less than 1 min compared with 120 min for the PET scan and a noncontrast CT acquisition. DECT can cost $300 to $500, whereas PET can cost $1,000 or more. The disadvantages of DECT are similar to those of PET/CT: it is a less accessible modality than single-energy CT and it requires similar radiation doses. Whereas there is an increasing number of DECT scanners available in the USA, compelling clinical uses have been lacking, unlike those for PET/CT, which has been shown to provide valuable additional clinical information.

In summary, we note that our results demonstrated that univariate analysis does not perform as well as multivariate analysis in terms of correlating quantitative DECT values to PET SUV_{max} in patients with PA. Additionally, multivariate analysis reveals that noncontrast images may contain important predictive information, an interesting finding that should be followed up in future studies with larger sample sizes. Enhanced DECT shows a moderate correlation with SUV_{max} when measured on the area of the tumor correlating to the highest SUV_{max}, or, if one wishes to avoid performing PET/CT altogether, when taking three measurements in the greatest

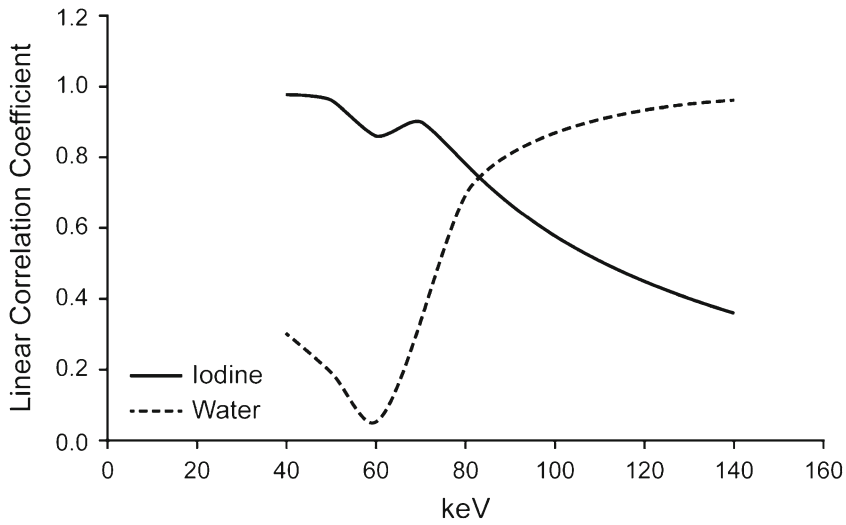

Fig. 5 Correlation of image value with iodine member of iodine–water basis pair for a typical region of interest

areas of tumor heterogeneity (which is almost as effective in mimicking PET). In the future, if these results are confirmed in larger studies and the interface for acquiring this information is simplified, DECT could serve as a useful complement or alternative to PET/CT imaging for PA.

Conclusion

We have demonstrated that DECT can, under certain conditions, serve as a surrogate for a PET scan in terms of estimating SUV_{max}. DECT thus has clinical potential as a surrogate for, or as a complement to, PET in patients with PA. In this case, DECT might be able to be used in place of PET in locations without access to a PET scanner, or to improve diagnosis and/or prognostication in centers with access to a PET scanner. Additionally, the future use of more complicated texture parameters may further improve the diagnostic and prognostic ability of DECT, and may help to investigate response to therapy for cancers where PET is presently used.

Conflict of Interest None.

References

1. National Comprehensive Cancer Network (NCCN). NCCN clinical practice guidelines in oncology: pancreatic adenocarcinoma [Internet]. Fort Washington (PA): National Comprehensive Cancer Network; 2011 Dec 7 [updated 2013 Apr 9; cited 2012 Aug 2012]. Available from: http://www.nccn.org/professionals/physician_gls/PDF/pancreatic.pdf
2. Montgomery DC, Peck EA, Vining GG. Introduction to linear regression analysis. 4th ed. Hoboken (NJ). Wiley-Interscience; c2006: p. 110
3. Pery C, Meurette G, Ansquer C, Frampas E, Regenet N: Role and limitations of 18F-FDG positron emission tomography (PET) in the management of patients with pancreatic lesions. Gastroenterol Clin Biol 34(8–9):465–474, 2010
4. Delbeke D, Martin WH: PET and PET/CT for pancreatic malignancies. Surg Oncol Clin N Am 19(2):235–254, 2010
5. Cameron K, Golan S, Simpson W, Peti S, Roayaie S, Labow D, Kostakoglu L: Recurrent pancreatic carcinoma and cholangiocarcinoma: 18F-fluorodeoxyglucose positron emission tomography/computed tomography (PET/CT). Abdom Imaging 36(4):463–471, 2011
6. Silva AC, Morse BG, Hara AK, Paden RG, Hongo N, Pavlicek W: Dual-energy (spectral) CT: applications in abdominal imaging. Radiographics 31(4):1031–1046, 2011
7. Graser A, Johnson TR, Bader M, Staehler M, Haseke N, Nikolaou K, Reiser MF, Stief CG, Becker CR: Dual energy CT characterization of urinary calculi: initial in vitro and clinical experience. Investig Radiol 43(2):112–119, 2008
8. Graser A, Johnson TR, Hecht EM, Becker CR, Leidecker C, Staehler M, Stief CG, Hildebrandt H, Godoy MC, Finn ME, Stepansky F, Reiser MF, Macari M: Dual-energy CT in patients suspected of having renal masses: can virtual nonenhanced images replace true nonenhanced images? Radiology 252(2):433–440, 2009
9. Macari M, Spieler B, Kim D, Graser A, Megibow AJ, Babb J, Chandarana H: Dual-source dual-energy MDCT of pancreatic adenocarcinoma: initial observations with data generated at 80 kVp and at simulated weighted-average 120 kVp. AJR Am J Roentgenol 194(1):W27–W32, 2010
10. Mileto A, Mazziotti S, Gaeta M, Bottari A, Zimbaro F, Giardina C, Ascenti G: Pancreatic dual-source dual-energy CT: is it time to discard unenhanced imaging? Clin Radiol 67(4):334–339, 2012
11. Schmid-Bindert G, Henzler T, Chu TQ, Meyer M, Nance Jr, JW, Schoepf UJ, Dinter DJ, Apfaltrer P, Krissak R, Manegold C, Schoenberg SO, Fink C: Functional imaging of lung cancer using dual energy CT: how does iodine related attenuation correlate with standardized uptake value of 18FDG-PET-CT? Eur Radiol 22(1):93–103, 2012
12. Hall M, Frank E, Holmes G, Pfahringer B, Reutemann P, Witten IH: The WEKA data mining software: an update. SIGKDD Explor 11(1): 10–18, 2009
13. Hastie T, Tibshirani R, Friedman J, editors. The elements of statistical learning: data mining, inference, and prediction. New York: Springer Science and Illustration Media, Inc.; c2001. Chapter 3, Linnear methods for regression; p. 41–78
14. Guyon I, Elisseeff A: An introduction to variable and feature selection. JMLR 3:1157–1182, 2003
15. Seo S, Doi R, Machimoto T, Kami K, Masui T, Hatano E, Ogawa K, Higashi T, Uemoto S: Contribution of 18F-fluorodeoxyglucose positron emission tomography to the diagnosis of early pancreatic carcinoma. J Hepatobiliary Pancreat Surg 15(6):634–639, 2008
16. Koyama K, Okamura T, Kawabe J, Nakata B, Chung KH, Ochi H, Yamada R: Diagnostic usefulness of FDG PET for pancreatic mass lesions. Ann Nucl Med 15(3):217–224, 2001
17. Delbeke D, Rose DM, Chapman WC, Pinson CW, Wright JK, Beauchamp RD, Shyr Y, Leach SD: Optimal interpretation of FDG PET in the diagnosis, staging and management of pancreatic carcinoma. J Nucl Med 40(11):1784–1791, 1999
18. Lee SM, Kim TS, Lee JW, Kim SK, Park SJ, Han SS: Improved prognostic value of standardized uptake value corrected for blood glucose level in pancreatic cancer using F-18 FDG PET. Clin Nucl Med 36(5):331–336, 2011
19. Haaga JR, Alfidi RJ, Zelch MG, Meany TF, Boller M, Gonzalez L, Jelden GL: Computed tomography of the pancreas. Radiology 120: 589–595, 1976
20. Sheedy 2nd, PF, Stephens DH, Hattery RR, MacCarty RL: Computed tomography in the evaluation of patients with suspected carcinoma of the pancreas. Radiology 124(3):731–737, 1977
21. Ros PR, Mortele KJ: Imaging features of pancreatic neoplasms. JBR-BTR 84(6):239–249, 2001
22. Drabycz S, Stockwell RG, Mitchell JR: Image texture characterization using the discrete orthonormal S-transform. J Digit Imaging 22(6):696–708, 2009
23. Zhang Y, Zhu H, Mitchell JR, Costello F, Metz LM: T2 MRI texture analysis is a sensitive measure of tissue injury and recovery resulting from acute inflammatory lesions in multiple sclerosis. Neuroimage 47(1):107–111, 2009
24. Goh V, Ganeshan B, Nathan P, Juttla JK, Vinayan A, Miles KA: Assessment of response to tyrosine kinase inhibitors in metastatic renal cell cancer: CT texture as a predictive biomarker. Radiology 261(1):165–171, 2011
25. Wang H, Guo XH, Jia ZW, Li HK, Liang ZG, Li KC, He Q: Multilevel binomial logistic prediction model for malignant pulmonary nodules based on texture features of CT image. Eur J Radiol 74(1):124–129, 2010
26. Yu H, Caldwell C, Mah K, Poon I, Balogh J, MacKenzie R, Khaouam N, Tirona R: Automated radiation targeting in head-and-neck cancer using region-based texture analysis of PET and CT images. Int J Radiat Oncol Biol Phys 75(2):618–625, 2009